

## Experimental and analytical assessment of lateral torsional buckling of laminated glass beams

Belis, Jan; Bedon, Chiara; Louter, Christian; Amadio, Claudio; Van Impe, Rudy

**DOI**

[10.1016/j.engstruct.2013.02.002](https://doi.org/10.1016/j.engstruct.2013.02.002)

**Publication date**

2013

**Document Version**

Final published version

**Published in**

Engineering Structures

**Citation (APA)**

Belis, J., Bedon, C., Louter, C., Amadio, C., & Van Impe, R. (2013). Experimental and analytical assessment of lateral torsional buckling of laminated glass beams. *Engineering Structures*, 51, 295-305. <https://doi.org/10.1016/j.engstruct.2013.02.002>

**Important note**

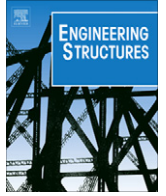
To cite this publication, please use the final published version (if applicable). Please check the document version above.

**Copyright**

Other than for strictly personal use, it is not permitted to download, forward or distribute the text or part of it, without the consent of the author(s) and/or copyright holder(s), unless the work is under an open content license such as Creative Commons.

**Takedown policy**

Please contact us and provide details if you believe this document breaches copyrights. We will remove access to the work immediately and investigate your claim.



# Experimental and analytical assessment of lateral torsional buckling of laminated glass beams



Jan Belis<sup>a,\*</sup>, Chiara Bedon<sup>b</sup>, Christian Louter<sup>c,1</sup>, Claudio Amadio<sup>b</sup>, Rudy Van Impe<sup>a</sup>

<sup>a</sup> Department of Structural Engineering – LMO, Ghent University, Technologiepark-Zwijnaarde 904, B-9052 Ghent, Belgium

<sup>b</sup> University of Trieste, Faculty of Engineering, Department of Civil Engineering and Architecture, Piazzale Europa n. 1, 34127 Trieste, Italy

<sup>c</sup> Delft University of Technology, Faculty of Architecture, Department of Building Technology, 2628 CR Delft, The Netherlands

## ARTICLE INFO

### Article history:

Received 30 October 2012

Revised 31 January 2013

Accepted 5 February 2013

Available online 8 March 2013

### Keywords:

Structural glass

Lateral torsional buckling

Buckling

Glass beam

Experiment

Analytical analysis

Initial geometrical imperfection

Laminated Glass

Equivalent torsional stiffness

## ABSTRACT

Due to their increasing use in contemporary architecture, the lateral torsional buckling performance of laminated structural glass beams represents a topic of great interest for researchers. Although several analytical models and design approaches have been recently proposed, various aspects complicate the realistic prediction of this phenomenon. Based on experimental results of a large campaign of lateral torsional buckling tests (55 laminated beams), the paper investigates analytically the effects of various mechanical (e.g. the stiffness of interlayer) and geometrical properties (e.g. initial twist, production tolerances) on the typical lateral torsional buckling response of laminated glass beams.

© 2013 Elsevier Ltd. All rights reserved.

## 1. Introduction

Stability issues are known to be of major importance for the proper design of loadbearing glass components and structures [1–9]. As far as stability of glass beams is concerned, several authors have already addressed lateral torsional buckling (LTB) and have proposed design approaches [2–4]. However, in spite of the latter, to date the influence of several parameters on the buckling resistance of glass beams has not always been fully understood. Regarding initial geometrical imperfections for instance, extensive experimental data is available about initial curvature [10], also known as global bow, but initial rotations of the beam's cross-section along its longitudinal axis, also known as twist, are usually not considered. Consequently, based on new data of 55 full-scale lateral torsional buckling experiments on laminated glass beams in combination with numerical modelling techniques, this contribution focuses on the importance of initial twist on the buckling behaviour of laminated glass beams. Particular attention is also dedicated to the effects of possible production tolerances in glass thicknesses. As shown by means of several experimental

and analytical comparisons, initial twist and real glass thicknesses can strongly influence the structural behaviour of laminated glass beams in buckling.

## 2. Materials and methods

### 2.1. Test specimens

Throughout the experimental campaign, a total of 55 laminated glass test specimens with two glass layers each had been tested, subdivided in 12 series. Differences between series are related to differences in interlayer materials (polyvinyl butyral (PVB) and SentryGlas<sup>(R)</sup> (SG)), glass type (annealed (AN), heat-strengthened (HS) and fully tempered (FT)), and geometrical parameters (thickness  $t$ , height  $h$  and ratio between total length  $L$  and height  $h$ ). All test specimens were characterized by a total length  $L = 3000$  mm. Nevertheless, due to beam restraints, the effective buckling length considered in calculations was  $L_0 = 2900$  mm. An overview of specimens is presented in Table 1.

### 2.2. Experimental methods

All experiments have been performed in laboratory conditions. Temperature registrations during the tests varied between 18.5 °C

\* Corresponding author. Tel.: +32 9 264 54 78; fax: +32 9 264 5838.

E-mail address: [jan.belis@UGent.be](mailto:jan.belis@UGent.be) (J. Belis).

<sup>1</sup> Present address: Steel Structures Laboratory (ICOM), École Polytechnique Fédérale de Lausanne (EPFL), GC B3 505, Station 18, CH-1015 Lausanne, Switzerland.

**Table 1**  
Overview of LG test specimens used during the experimental campaign. All specimens had polished edges. Glass types AN, HS and FT represent annealed, heat-strengthened and tempered glass, respectively.

Series	Glass type	Interlayer material <sup>a</sup>	Length $L$ (mm) <sup>b</sup>	Height $h$ (mm)	Length/height $L/h$ (-)	Glass thickness $t$ (mm)	Number of specimens	Origin
B	AN	PVB	3000	120	25	2 × 6	4	EU
A		PVB	3000	120	25	2 × 8	4	EU
C		PVB	3000	150	20	2 × 6	4	EU
D		PVB	3000	150	20	2 × 8	4	EU
F		PVB	3000	300	10	2 × 10	5	Asia
S	HS	PVB	3000	300	10	2 × 10	5	Asia
E	FT	PVB	3000	200	15	2 × 6	8	EU
T		PVB	3000	300	10	2 × 10	5	Asia
G		SG	3000	200	15	2 × 6	4	EU
I		SG	3000	200	15	2 × 8	4	EU
H		SG	3000	300	10	2 × 6	4	EU
J		SG	3000	300	10	2 × 8	4	EU
							55	

<sup>a</sup> Interlayer thickness was 1.52 mm for PVB and 2.28 mm for SG.

<sup>b</sup> Due to beam restraints, the design buckling length assumed in all the calculations proposed in this work is  $L_0 = 2900$  mm.

and 20.5 °C. Consequently, with good approximation a constant operating temperature of 19.5 °C will further be assumed for the analytical predictions of all tests.

### 2.2.1. Initial shape imperfection measurements

Initial shape imperfections in general, and global bow in particular, are generally known to be of importance in many instability problems, including lateral torsional buckling. Consequently, prior to the actual buckling tests all test specimens were thoroughly measured to obtain accurate values of the global bow, both in terms of shape and amplitude. A custom-made measurement setup was used, in which a linear variable differential transducer (LVDT) was moved at constant speed along the full length of the specimens while registering the relative distance to a reference rail at each measurement location. Obviously, initial shape imperfections of the reference rail itself were filtered out not to influence the results. A detailed description of the full measurement method and equipment has been reported on earlier and will therefore not be repeated here [10].

### 2.2.2. Lateral torsional buckling test setup

The lateral torsional buckling test setup is illustrated in Fig. 1 and consisted of a large steel frame basis on which (1) custom-made supports, (2) load system and (3) data-acquisition can be mounted according to the test specimen geometry. These three components are subsequently discussed below in more detail. As depicted in Figs. 1 and 2, an orthogonal coordinate system is used in which the directions of X, Y and Z-axes correspond to the horizontal direction perpendicular to the test specimen, the vertical direction, and the longitudinal direction of the test specimen, respectively.

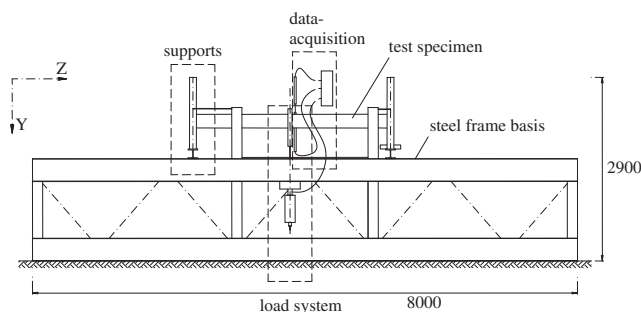


**Fig. 1.** General overview of lateral torsional buckling test setup. All dimensions are in mm.

Firstly, the supports are designed as fork bearings which restrain rotations about the longitudinal axis (i.e. Z-axis) but enable rotations about the other axes (X- and Y-axis). However, to be in line with common theoretical assumptions, it is essential to avoid friction during rotations. Consequently, high-quality bearings and low friction mylar interlayers were used to minimize friction during rotations about the Y- and X-axis, respectively (see Fig. 2). According to good practice, 2 mm rubber or aluminium contact strips were additionally used at the load introduction points to avoid high local stress concentrations in the glass.

Secondly, loads were indirectly introduced at mid-span by a hydraulic jack, pulling downwards a cross-beam, which was positioned on top of the test specimen. However, to be in good agreement with analytical solutions, which usually assume a gravity load, it is essential that the load remains vertical during the test. This is a challenge for the test setup, because the load introduction point at mid-span will rotate and laterally displace due to torsion and out of plane bending of a test specimen subjected to LTB. To enable rotations at the load introduction point, loads were introduced on the upper edge of the beam by means of a sharp wedge, which could freely rotate about the longitudinal axis in a gutter (see Fig. 3). To enable lateral displacements, the hydraulic jack was mounted on a rolling device so that it could move in lateral direction to follow the out-of-plane movement of the load introduction point as the test specimen was bending out of plane during the buckling test. The test procedure was displacement controlled.

Finally, data acquired from the tests consisted of the applied load, measured by a load cell, and lateral and vertical displacements of the upper edge of the test specimens near mid-span, measured by LVDTs, each obtained at a rate of one measurement per second.

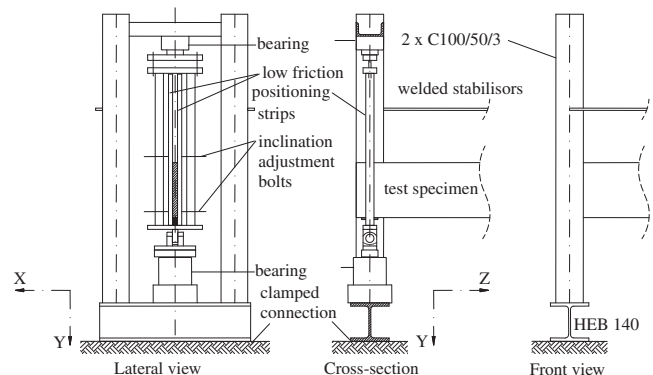


**Fig. 2.** Details of supports, which enable free rotations about X-axis and Y-axis.

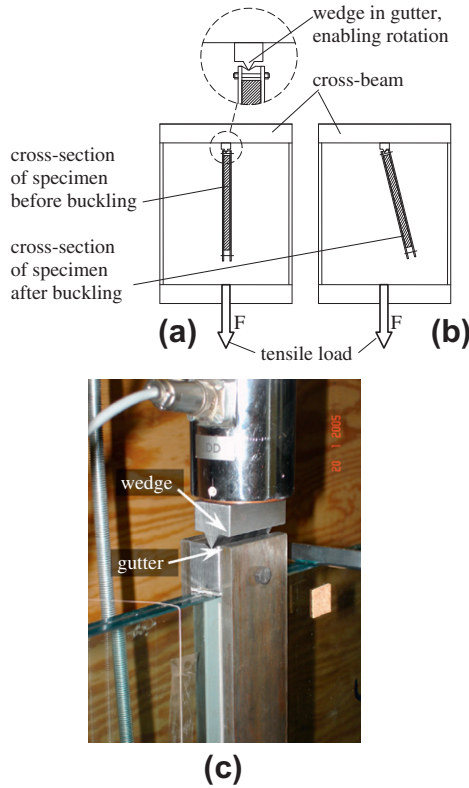


**Fig. 3.** Details of loading system. (a) Original situation: specimen cross-section still in quasi-vertical position; (b) buckled situation: rotated specimen cross-section about longitudinal axis; load still in vertical position (relative rotation at load introduction point enabled by wedge and gutter); (c) detailed view of load introduction.

### 2.2.3. Thickness measurements

After the buckling tests, 1.1 m long parts of the buckled and broken beams were recovered to perform subsequent bending tests to determine the edge strength of the used glass, as illustrated in Fig. 4. For obvious reasons, this was only done for specimens composed of annealed glass. Although the strength tests are not relevant for this contribution, the precise measurements of the geometry of those specimens made at that occasion are of interest here. The height  $h$  and total laminated thickness  $t_{tot}$  of each specimen was determined according to EN 1288-3 2000 as the average of four measurements on each specimen, at locations indicated in Fig. 4. A caliber with an accuracy of 0.01 mm was used for all measurements. As the thickness  $t$  of individual glass sheets could not be measured prior to lamination, the latter was determined as half the value obtained by subtracting the nominal interlayer thickness (Table 1) from the total measured laminated thickness  $t_{tot}$ .

## 2.3. Theoretical methods

### 2.3.1. Southwell plot

Fundamentals of stability theory are widely spread, e.g. [11–13], and are therefore not repeated here. However, less known is the so-called Southwell plot, which provides a very useful procedure to derive the theoretical buckling load from buckling experiments on geometrically similar test specimens with small initial shape imperfections (global bow) [14–16]. The basic expression derived by Southwell is presented in

$$\frac{u}{F^i} = \frac{1}{F_{cr}^i} \cdot u + \frac{u_0}{F_{cr}^i} \quad (1)$$

In Eq. (1),  $u$  represents the maximum value of the lateral displacement (i.e. at mid-span),  $u_0$  its initial value,  $F$  is the applied load

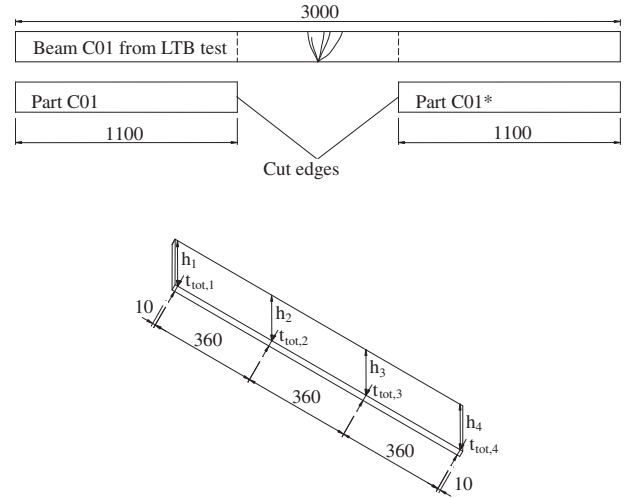


**Fig. 4.** Locations taken into account, in annealed glass specimens, for the measurements of their real total laminated thickness  $t_{tot}$  and height  $h$ .

and  $F_{cr}$  is the elastic buckling load. The exponent  $i$  needs to be chosen such that experimental results are approximately linear. Subsequently, if  $u/F$  is plotted as a function of  $u$ ,  $F_{cr}$  can be derived from the slope  $1/F_{cr}$  of the linear curve. Consequently, the elastic buckling load can be obtained from experimental values for  $u$  and  $F$ , and is independent from the initial shape imperfection  $u_0$ . For practical applications,  $F_{cr}$  is defined as the inverse of the slope of the best fitting linear curve through the experimentally obtained data points.

### 2.3.2. Lateral torsional buckling analysis

In accordance with suggestions of EC3 [17], the elastic critical load of each laminated glass beam can be calculated by means of the classical formulation:

$$F_{cr} = 1.365 \cdot \frac{4\pi^2 E J_y}{L_0^3} \cdot \left\{ \sqrt{\frac{L_d^2 G J_t}{\pi^2 E J_y} + \left(0.553 \cdot \frac{h}{2}\right)^2} - 0.553 \cdot \frac{h}{2} \right\}, \quad (2)$$

in which  $E J_y$  and  $G J_t$  express respectively the flexural and torsional stiffness of the beam,  $L_0$  is the effective buckling length (Table 1) and  $h$  its height. Evidently, Eq. (2) primarily applies to monolithic beams, but with particular attention it can also be used to predict the elastic buckling load of laminated glass beams. In this work,  $E J_y$  has been calculated for each specimen by means of the equivalent thickness approach already applied to 2-layer laminated glass columns and validated in [18], with  $E = 70000 \text{ N/mm}^2$  the Young's modulus of glass. Similarly  $G J_t$ , has been determined for each beam by means of the formulations derived from classical theory of sandwich elements and successfully used for the analysis of laminated glass units in [2,19], with  $G = 28455 \text{ N/mm}^2$  the shear modulus of glass. In this manner, the mechanical properties of the adopted interlayer (e.g. the shear modulus  $G_{int}$ ), are directly included in the term  $G J_t$ . More specifically, interlayer shear modulus values used in the analyses are chosen as accurately as possible by combining the exact load duration of each test (see Table A.1) with detailed PVB and SG data available in literature [21,3]. As a result, analytical calculations for laminated glass beams in well-defined conditions of temperature and load-duration can be performed on a monolithic glass section of equivalent flexural and torsional properties.

Further analytical calculations have also been performed to predict the typical out-of-plane response of the examined beams. As known, in the study of the stability behaviour of a beam in bending, the critical buckling load represents a useful parameter for the estimation of its buckling strength. Nevertheless, it does not

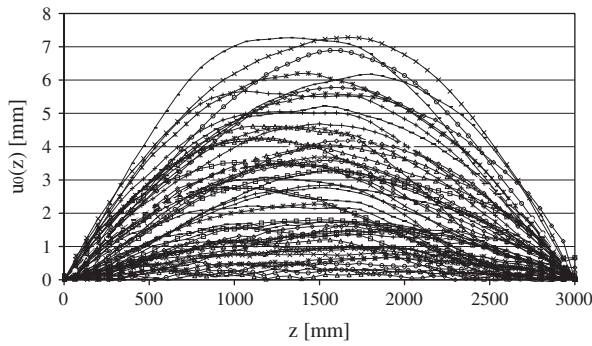


Fig. 5. Plots of initial lateral displacements as a function of the length of the laminated glass specimens, yielding a general overview of shape and amplitude of initial shape imperfections (global bow).

constitute enough detailed information to investigate in depth the structural response of the beam. In this context, the knowledge of its typical load–displacement response represents an interesting aspect to be investigated. For this purpose, a second order formulation has been used to predict analytically the load–displacement relationship of each specimen. Comparisons with experimental results have been performed by using the equation [20]:

$$u(x) = \frac{c_1 \cdot \frac{G_t}{E_y} \cdot M_z \theta_0 + c_1^2 \cdot \frac{M_z^2}{E_y} \cdot u_0}{GJ_t \cdot \left(\frac{\pi}{L_0}\right)^2 - c_1^2 \cdot \frac{M_z^2}{E_y} + c_2 \cdot M_z z_p \left(\frac{\pi}{L_0}\right)^2} \cdot \sin\left(\frac{\pi}{L_0} x\right). \quad (3)$$

Eq. (3) well expresses the amplitude of the horizontal displacement at the barycentrical axis of a general section  $x$  ( $0 \leq x \leq L_0$ ), for a beam with effective buckling length  $L_0$  and subjected to a bending moment  $M_z$  due to the applied load  $F$ . In it, the coefficients  $c_1$  and  $c_2$  depend on the loading condition ( $c_1 = 0.7026$  and  $c_2 = 0.8693$  in presence of a concentrated load  $F$  at mid-span). In addition,  $\theta_0$  and  $u_0$  respectively denote the maximum amplitude of the initial rotational imperfection (assumed as a sinusoidal rotational imperfection having maximum amplitude at mid-span) and the maximum amplitude of the initial bow affecting each beam. Based on experimental measurements and results of previous works [9],  $u_0$  is considered in this contribution as the maximum initial deflection experimentally measured along each specimen (Table A.1). Finally, in Eq. (3) the term  $z_p$  denotes the distance between the applied load

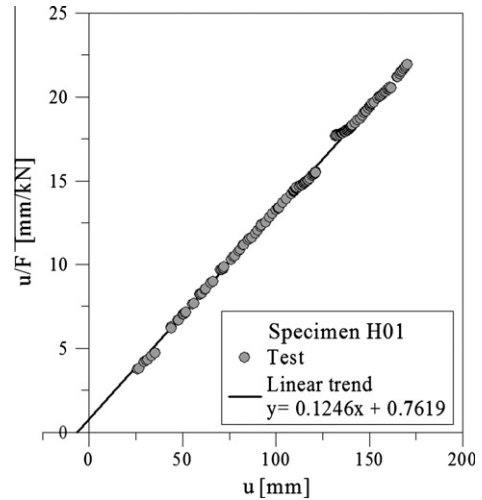


Fig. 6. Example Southwell plot, in this case of specimen H01.  $u$  represents lateral displacements at mid-span;  $F$  is the applied concentrated load.

$F$  and the barycentrical axis of each beam, whereas  $EJ_y$  and  $GJ_t$  have been previously defined.

To perform a series of first comparisons between experimental and analytical predictions, the critical load of each beam has been estimated analytically by means of Eq. (2).

Successively, also the analytical load–displacement relationships given by Eq. (3) have been compared to experimental results.

### 3. Experimental results

#### 3.1. Global bow

As expected and illustrated in Fig. 5, the shape of the initial imperfections was generally very similar to a half sinus wave [10]. Maximum values of imperfection amplitudes, which mostly did not appear exactly at – though close to – mid-span, are listed in Table A.1. Measured imperfections for the examined 55 specimens resulted to be extremely variable, for beams constituting a same series of specimens as well as for all the beams in general

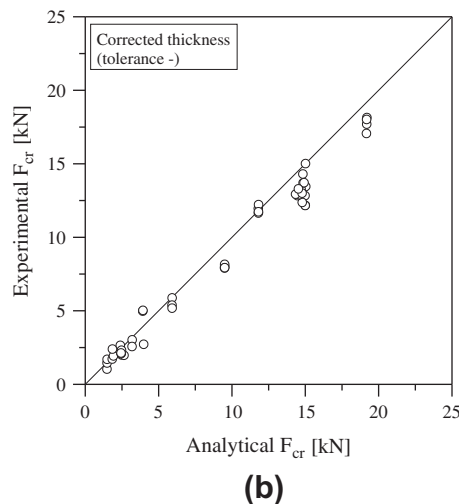
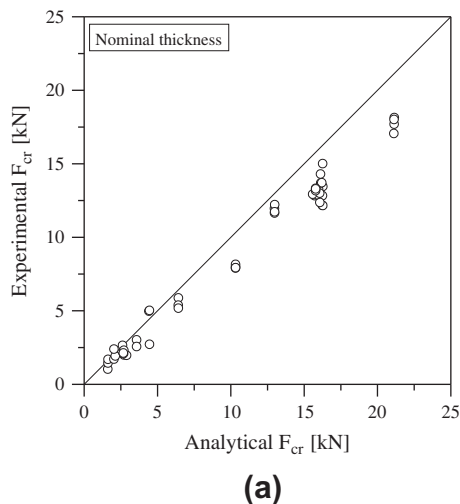
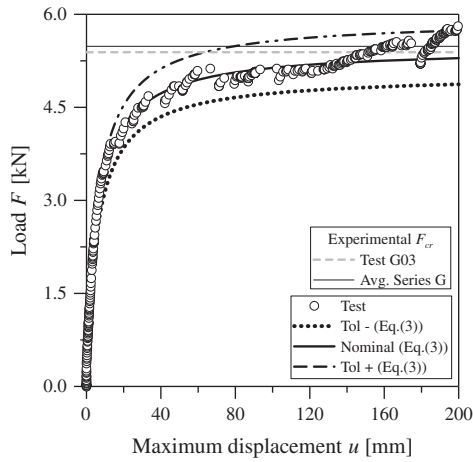


Fig. 7. Comparison of experimental and analytical (Eq. (2)) elastic buckling loads of all specimens. (a) Nominal thickness; (b) corrected thickness.



**Fig. 8.** Good correlation of experimental and analytical results (in this case specimen G03). Comparison between experimental load–displacement path and analytical predictions (nominal thickness, corrected thickness).

(average amplitude 3.116 mm; max. 7.282 mm for specimen E07; min. 0.250 for specimen S04).

### 3.2. Results of geometry measurements

Average values for the height and thickness of the investigated specimens are obtained according to the method described in Section 2.2.3 and summarized in Table B.1.

### 3.3. Elastic buckling loads obtained by Southwell plots

Using Southwell plot theory explained in Section 2.3, the elastic buckling load of the test specimens was determined. In Eq. (1) a value  $i = 1$  is used to derive the elastic buckling load from the experiments; its correctness can easily be checked by visually evaluating the linearity of the obtained plot, as illustrated in Fig. 6 for e.g. specimen H01. The elastic critical load was estimated experimentally only for 48 specimens, as clarified in Table C.1. Subsequently, according to Eq. (1), the elastic buckling load  $F_{cr}$  was determined by the inverse of the slope of the best fitting linear curve through the experimentally obtained data points. An overview of the resulting values for  $F_{cr}$  is listed in Table C.1.

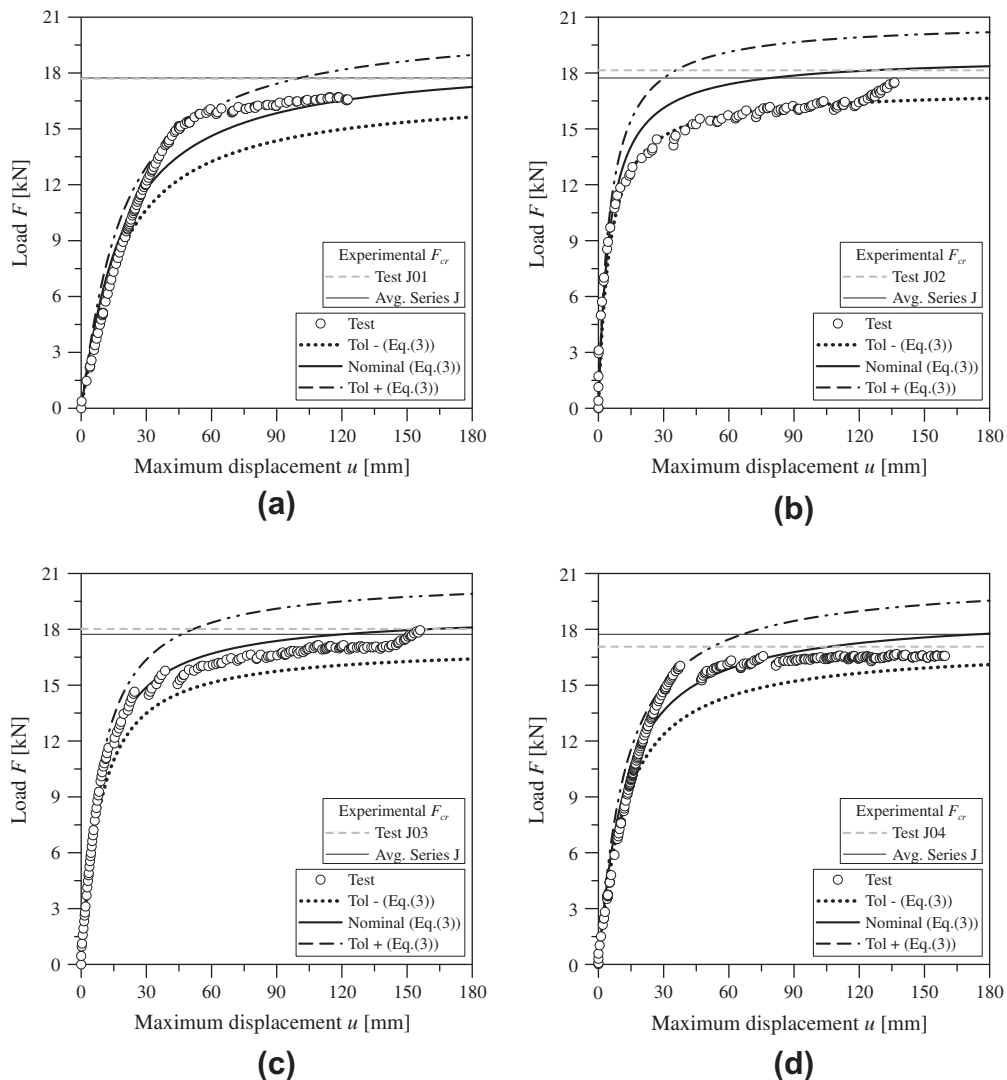


**Fig. 9.** Good correspondence of experimental and analytical results (in this case specimens of Series J). Comparison between experimental load–displacement paths and analytical predictions (nominal thickness, corrected thickness). Plots: (a) specimen J01; (b) specimen J02; (c) specimen J03; (d) specimen J04.

## 4. Discussion and comparison of experimental and analytical results

### 4.1. Elastic buckling load

Experimental critical loads were compared with analytical predictions obtained by means of Eq. (2). The shear stiffness  $GJ_t$  of each laminated beam was estimated by taking into account the average temperature registered during tests (19.5 °C) and the exact duration of each experiment. The shear modulus  $G_{int}$  of each PVB or SG interlayer was then extrapolated from master curves available in literature [3,21]. Further details can be found in Table A.1.

In the first series of analytical calculations, the nominal thicknesses  $t$  and heights  $h$  were taken into account for each laminated glass beam (Table 1). The experimental critical loads of 48 specimens were considered for comparisons (Fig. 7a and Table C.1). For most beams tested, there is a reasonable correspondence between the analytical and experimental results (Fig. 7a). Nevertheless, the analytical critical load is generally higher than the experimental one (Table C.1). In particular, the average ratio between experimental and analytical predictions  $R = F_{cr}^{exp}/F_{cr}^{an}$  is equal to 0.847, and only for five beams the analytical estimation of  $F_{cr}$  is conservative (specimens B04, C03, D03, D04, E02).

Based on available experimental measurements, further analytical calculations were performed considering in Eq. (2) the real thickness and height of each glass sheet (Series A, B, C, D, and F; Table B.1). The replacement of nominal dimensions with effective ones affects significantly the results of analytical calculations (Table C.1), and in general better results are obtained ( $R = 0.920$ ). Major improvements in the analytical estimation of  $F_{cr}$  depend on the thickness of each glass sheet and slightly on the height of the beams. Nevertheless, measurements of experimental dimensions are not generally available in the design of structural glass elements (in this work, the real dimensions of only 16 specimens were available), and often, due to production process, they are rather variable.

Because of these reasons, further calculations have been performed with a thickness corresponding to the lower glass production tolerance limit, which for economic reasons is usually targeted as good as possible by glass manufacturers. According to EN572-8 [22], production tolerances of float glass depend on the nominal glass thickness ( $\pm 0.2$  mm in case of glass with a nominal thickness of 6 mm,  $\pm 0.3$  mm for glass thicknesses of 8 mm or 10 mm). Detailed results of these further predictions are proposed for all 48

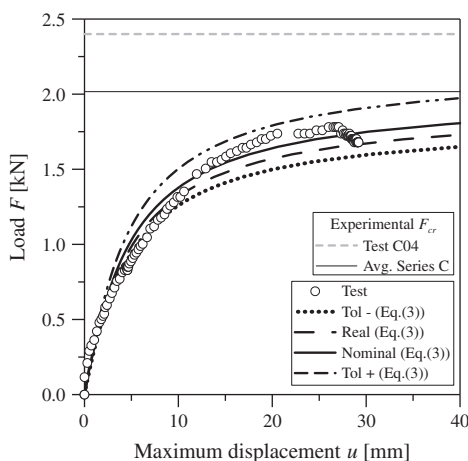


Fig. 10. Poor correspondence of experimental and analytical results (in this case of specimen C04). Comparison between experimental load–displacement path and analytical predictions (nominal thickness, real thickness, corrected thickness).

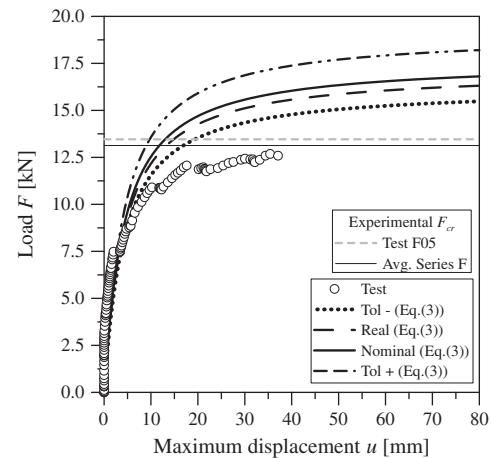


Fig. 11. Poor correspondence of experimental and analytical results (in this case of specimen F05). Comparison between experimental load–displacement path and analytical predictions (nominal thickness, real thickness, corrected thickness).

specimens in Table C.1. As expected, the assumption of a positive production tolerance for glass thickness (Tol+) manifests in non-conservative analytical predictions ( $R = 0.784$ ). Contrarily, the use of a negative production tolerance (Tol–) results in a good agreement for most of the examined beams. Generally this assumption manifests in a more conservative prediction of the critical buckling load (Table C.1 and Fig. 7b;  $R = 0.928$ ) and calculations for nine beams (only five with glass nominal thickness) provide safe results. In addition, calculations for the Exp./Tol– ratio of four further beams (no beams, if glass nominal thickness is taken into account) result in a value approximately equal to 1 (specimens B03, G02, I02, I04). Calibrations to numerical FE results provided in [18,19] demonstrate the accuracy of the used analytical approach. Consequently, since experimental results are rather variable due to several factors (e.g. number of specimens, type of glass, possible technical problems occurred during test measurements, etc.), when real measurements are not available, a negative production tolerance (Tol–) should be used instead of nominal thicknesses.

### 4.2. Load–displacement path

Further detailed investigations have been dedicated to the typical load–displacement path of the 48 examined specimens and Eq. (3) has been used to predict their out-of-plane response. Up till now, initial rotation of the cross-section at half length of the beams has been neglected in the analysis, as it was not measured experimentally. However, calculations demonstrated that the accuracy of the analytical predictions can be further improved by calibrating this parameter to the experimentally obtained load–displacement curves. Generally, the initial rotational imperfection (and thus the first numerator term of Eq. (3)), even if of small amplitude, strongly affects the slope of analytical load–displacement path and puts forward the failure of the beam. Calibrations of rotational imperfections for the 48 examined specimens resulted in a small rotation, having average amplitude of 0.0064 rad. Details for the calibrated initial rotational amplitudes can be found in Table A.1.

To avoid a plethora of graphs and data, in this section only few relevant examples are proposed and commented, whereas further comparisons between experimental and analytical load–displacement paths are collected in Table B.1. In general, as expected, the quality of an experimental  $F$ – $u$  plot depends on the amount of available test data. Additional technical (e.g. possible measurements problems during tests) and mechanical parameters (e.g. the amplitude of rotational imperfection  $\theta_0$ ) can complicate a real-

istic analytical prediction of the flexural torsional behaviour of a laminated glass beam. In these hypotheses, specimen G03 is presented in Fig. 8 as a good example test result, since well representative of the complete flexural torsional response of the examined beam. Experimental results are compared in Fig. 8 with analytical  $F-u$  curves obtained by assuming in Eq. (3), respectively, the nominal glass thickness and a thickness corrected with a positive (Tol+) or negative (Tol-) production tolerance. An amplitude of 0.003 rad is assumed for the calibrated rotational imperfection  $\theta_0$  (Table A.1). In the same figure, also two values of critical load are proposed for the beam G03, experimentally estimated as the buckling load of the specimen and the average critical load of Series G. To preserve the understanding of Fig. 8, the corresponding analytical buckling loads given by Eq. (2) and summarized in Table C.1 for the beam G03 with various glass thicknesses are not illustrated. Nevertheless, as expected, each one of these critical loads  $F_{cr}$  approximately coincides with the asymptotic value of the corresponding  $F-u$

curves proposed in Fig. 8. As shown, there is a very good correspondence between experimental and analytical values of the lateral displacements as a function of the load, and test results are comprised between a lower limit curve (Tol-) and an upper limit curve (Tol+).

Further good correlations between test results and analytical predictions are also proposed in Fig. 9, for the specimens of Series J. Also in these examples the response of specimens (especially J01, J03 and J04) agrees well with analytical predictions obtained for the beams with nominal glass thicknesses. Again, the experimental path is comprised between the lower (Tol-) and upper (Tol+) limit curves. In addition, by comparing the initial slope of curves proposed in Fig. 9a and d, it is possible to notice the effects of calibrated rotational imperfections on the out-of-plane response of specimens (in order: 0.020 rad, 0.004 rad, 0.010 rad and 0.012 rad).

Comparisons performed for all the examined specimens resulted in several good agreements (Fig. D.1). However, for a limited

**Table A.1**

Amplitude of measured initial imperfection, calibrated initial rotation, duration of experiments and corresponding shear modulus adopted in calculations for the interlayer.

Series	Test	$u_0$ (mm)	$L_0/u_0$	$\theta_0$ (rad)	Duration (min s)	$G_{int}$ (N/mm <sup>2</sup> )
A	03	3.273	886	0.009	2.54	1.169
	04	4.050	716	0.010	2.51	1.170
B	02	2.281	1271	0.000	7.52	1.087
	03	6.892	421	0.007	3.20	1.162
	04	2.843	1020	0.015	2.12	1.181
C	02	3.274	886	0.000	2.17	1.181
	03	1.155	2511	0.012	1.23	1.694
	04	1.802	1609	0.008	1.55	1.186
D	01	1.200	2416	0.001	1.41	1.190
	03	4.568	635	0.001	6.34	1.108
	04	3.586	809	0.010	2.06	1.183
E	01	5.052	574	0.002	7.52	1.087
	02	2.213	1310	0.000	22.49	0.930
	04	5.776	502	0.003	9.18	1.063
	05	3.581	810	0.020	1.47	1.188
	06	4.254	682	0.015	1.19	1.813
	07	7.282	398	0.006	6.42	1.106
	08	5.593	519	0.004	3.23	1.161
	04	2.779	1044	0.002	5.41	85.350
G	02	5.664	512	0.005	4.32	85.540
	03	7.274	399	0.003	8.50	84.840
	04	2.779	1044	0.002	5.41	85.350
	04	6.176	470	0.013	6.25	85.230
H	01	6.204	467	0.003	7.08	85.120
	02	4.233	685	0.003	6.17	85.120
	03	4.685	619	0.004	9.04	84.810
	04	6.176	470	0.013	6.25	85.230
I	01	3.475	835	0.003	10.52	84.520
	02	2.771	1046	0.006	9.03	84.810
	03	4.229	686	0.009	6.17	85.260
	04	3.496	830	0.004	7.55	84.990
J	01	5.223	550	0.020	6.41	85.190
	02	4.175	695	0.004	3.58	85.63
	03	1.563	1855	0.010	8.18	84.930
	04	4.613	629	0.012	11.03	84.500
F	01	0.960	3021	0.005	2.33	1.175
	02	0.960	3021	0.006	2.54	1.169
	03	0.500	5800	0.009	1.58	1.183
	04	1.490	1946	0.010	2.17	1.180
	05	1.730	1676	0.005	2.03	1.184
S	01	1.740	1667	0.005	6.49	1.104
	02	0.550	5273	0.003	14.29	0.976
	03	1.460	1986	0.006	5.43	1.123
	04	0.250	11,600	0.006	8.44	1.072
	05	1.00	2900	0.003	5.20	1.129
T	01	0.690	4203	0.007	11.12	1.031
	02	0.290	2900	0.007	21.48	0.931
	03	1.370	2117	0.004	3.43	1.156
	04	0.990	2929	0.005	7.08	1.101
	05	0.330	8788	0.004	5.18	1.001

**Table B.1**  
Average values of height and thickness of investigated annealed glass test specimens.

Specimen	$t_{mean}$ (mm)	$h_{mean}$ (mm)	$h_{front\ sheet}^a$ (mm)	$h_{back\ sheet}^a$ (mm)
A 02 <sup>b</sup>	17.16	120.40	–	–
A 02*	17.17	120.38	–	–
A 03	17.17	119.89	–	–
A 03*	17.16	119.91	–	–
A 04	17.15	118.66	–	–
A 04*	17.15	119.21	–	–
B 01 <sup>b</sup>	13.32	120.26	–	–
B 01*	13.31	120.45	–	–
B 02	13.33	120.89	–	–
B 02*	13.35	120.85	–	–
B 03	13.32	120.38	–	–
B 03*	13.30	120.64	–	–
B 04	13.34	120.08	–	–
B 04*	13.32	120.92	–	–
C 01 <sup>b</sup>	13.28	150.02	–	–
C 01*	13.30	149.28	–	–
C 02	13.28	149.18	–	–
C 02*	13.29	148.93	–	–
C 03	13.32	149.33	–	–
C 03*	13.32	148.82	–	–
C 04	13.31	150.00	–	–
C 04*	13.34	150.11	–	–
D 01	17.27	149.04	–	–
D 01*	17.24	148.78	–	–
D 02	17.15	148.85	–	–
D 02*	17.08	149.06	–	–
D 03 <sup>b</sup>	17.15	148.12	–	–
D 03*	17.18	147.82	–	–
D 04	17.16	146.91	–	–
D 04*	17.17	147.35	–	–
F 01	21.29	–	300.53	301.16
F 01*	21.37	–	299.18	300.82
F 02	21.12	–	302.07	301.21
F 02*	21.14	–	300.49	300.32
F 03	21.32	–	300.41	300.16
F 03*	21.23	–	300.26	300.55
F 04	21.38	–	301.84	299.94
F 05	21.27	–	301.21	300.82

<sup>a</sup> In contrast to the other series listed in this table, the glass edges of Series F had been laminated only after the edges of each individual glass sheet had been polished separately. Consequently, the height of front and back glass sheet differs.

<sup>b</sup> Specimens have been measured before testing, but no valid LTB test result was obtained (see Table C.1).

number of specimens, the correspondence between analytical and experimental load–displacement paths is rather poor. In few of those cases (specimens C04, D03, D04), compared to the experimental values, the elastic buckling load typically overestimates the analytically determined value, as for example proposed in Fig. 10 for specimen C04. A similar effect is typical of annealed specimens, as noticed in performing tests. Since extremely brittle and characterized by a well-known limited tensile strength, specimens composed of annealed glass (Series A, B, C and D) prematurely cracked before reaching their elastic lateral–torsional critical load. Consequently, few test results available for Southwell plots did not result in an accurate prediction of  $F_{cr}$ . Nevertheless, the experimental load–displacement path proposed for specimen C04 (Fig. 10) is in any case comprised within the upper (Tol+) and lower (Tol–) limit predictions. To be conservative, calculations should be generally performed by taking into account the lower production tolerance. Finally, analytical comparisons allowed to notice that for specimens of Series F, S and T (10 mm thick glass sheets) the analytical formulations provided by Eqs. (2) and (3) tend to overestimate their real buckling strength, as highlighted in Fig. 11 for beam F05. Although the correspondence between the initial slope of analytical  $F$ – $u$  plots and test results is good, neither the negative production tolerance (Tol–) provides an accurate estimation for  $F_{cr}$  ( $R = 0.893$  for Series F, S and T).

This unexpected observation may be explained by a difference in glass origin (Table 1). As the manufacturer of Series F, S and T was not a European-based company, it is likely that these series were not produced according to European standards, consequently larger tolerances may have been applicable. A backward calibration calculation of the actual glass thickness would yield an average tolerance of 0.7 mm (average value of calibrations performed on 15 specimens of Series F, S, and T), which is significantly larger than 0.3 mm as prescribed in Europe [22] for glass with a nominal thickness of 10 mm.

Undoubtedly, the corrected tolerance proposed in this work for 10 mm thick glass specimens strongly depends on the number and quality of available test results. Also calibrated tolerances for 6 mm (0.408 mm) and 8 mm (0.369 mm) glass thicknesses slightly exceed the production tolerances actually prescribed in [22]. Nevertheless, this finding should be opportunely taken into account in calculations and it could constitute a starting point for further detailed investigations.

## 5. Conclusions

Results of lateral torsional buckling tests performed on 55 PVB and SG laminated glass beams were presented and discussed in this contribution. As known, the elastic buckling load represents an important parameter for the definition of the effective strength of specimens. However, in performing an accurate and realistic investigation of the out-of-plane behaviour of laminated glass beams, also their load–displacement response should be opportunely analyzed. Based on analytical models available in literature, test results were compared with analytical predictions and the effects of various mechanical (e.g. the shear stiffness of the interlayer) and geometrical properties (e.g. the production tolerances for glass thickness, the amplitude of initial imperfection) were deeply investigated. The most important conclusions are listed below.

1. The type of glass is an important factor that should be carefully taken into account in the interpretation of test results. In this work, as expected, annealed glass specimens cracked prematurely due to their limited tensile strength; consequently, based on few available test results, estimations for the elastic buckling loads could be often not accurate.
2. Commonly, buckling tests are performed on glass beams neglecting that an initial rotation (even if of small amplitude) can be present in specimens. As highlighted in the paper, this initial twist should be always taken into account in the analysis of laminated glass beams, since it could put forwards their failure.
3. Based on production tolerances proposed by standards for the analysis of structural glass elements, further calculations have been proposed in this contribution. Since measured thicknesses are not generally available to designers, conservative calculations should be always performed assuming for glass the lower negative tolerance.
4. Experimental load–displacement paths can be in general predicted, with good accuracy, by means of equivalent thickness analytical approaches available in literature. In addition, for specimens with no optimal correspondence with analytical plots, test results are commonly comprised between a lower analytical curve (Tol–) and an upper analytical curve (Tol+).
5. Finally, it should be noted that the above mentioned conclusions have been derived from a thorough comparison of experimental and analytical results. A new design philosophy, taking all the above mentioned considerations into account, has yet to be developed in future studies.

**Table C.1**

Elastic critical loads obtained by experiments and analytical calculations, assuming for glass sheets the nominal thicknesses, the real thicknesses measured during tests, and thicknesses corrected by adding (Tol+) or subtracting (Tol−) the tolerance given in standards.<sup>a</sup>

Series	Test	Critical load (kN)					
		Experimental	Analytical (Eq. (2))				Exp./Tol−
			Nominal	Measured	Tolerance+	Tolerance−	
A	03	3.027	3.571	3.337	3.930	3.195	0.947
	04	2.573	3.571	3.319	3.919	3.186	0.808
	Avg.	2.800	3.571	3.328	3.924	3.190	0.878
B	02	1.036	1.608	1.554	1.771	1.476	0.702
	03	1.452	1.620	1.551	1.779	1.483	0.979
	04	1.702	1.623	1.560	1.783	1.486	1.145
	Avg.	1.397	1.617	1.555	1.778	1.482	0.942
C	02	1.719	2.026	1.908	2.200	1.836	0.936
	03	1.931	2.117	2.010	2.299	1.919	1.006
	04	2.400	2.027	1.939	2.216	1.850	1.297
	Avg.	2.016	2.056	1.952	2.239	1.868	1.080
D	01	2.725	4.451	4.221	4.891	3.979	0.685
	03	4.980	4.410	4.092	4.816	3.918	1.271
	04	5.033	4.448	4.103	4.830	3.929	1.281
	Avg.	4.246	4.437	4.139	4.846	3.942	1.079
E	01	2.111	2.676	–	2.922	2.443	0.864
	02	2.653	2.614	–	2.854	2.386	1.112
	04	2.134	2.667	–	2.913	2.435	0.876
	05	2.000	2.712	–	2.961	2.476	0.808
	06	1.977	2.888	–	3.153	2.639	0.749
	07	2.092	2.683	–	2.930	2.450	0.854
	08	2.320	2.703	–	2.952	2.468	0.940
	Avg.	2.184	2.706	–	2.955	2.471	0.884
G	02	5.879	6.421	–	6.949	5.919	0.993
	03	5.388	6.413	–	6.940	5.912	0.911
	04	5.184	6.419	–	6.947	5.917	0.876
	Avg.	5.484	6.417	–	6.945	5.916	0.927
H	01	8.026	10.319	–	11.183	9.499	0.845
	02	8.163	10.319	–	11.183	9.499	0.859
	03	7.911	10.315	–	11.179	9.496	0.833
	04	7.937	10.320	–	11.185	9.501	0.835
	Avg.	8.009	10.318	–	11.182	9.499	0.843
I	01	11.962	12.970	–	14.219	11.794	1.014
	02	11.655	12.977	–	14.227	11.800	0.988
	03	12.225	12.989	–	14.240	11.811	1.035
	04	11.737	12.982	–	14.232	11.805	0.994
	Avg.	11.895	12.979	–	14.229	11.802	1.008
J	01	17.699	21.132	–	23.201	19.186	0.922
	02	18.149	21.145	–	23.215	19.198	0.945
	03	18.018	21.125	–	23.193	19.180	0.939
	04	17.065	21.112	–	23.179	19.169	0.890
	Avg.	17.733	21.128	–	23.197	19.183	0.924
F	01	12.837	16.247	15.854	17.632	14.979	0.857
	02	12.180	16.232	15.440	17.651	14.995	0.812
	03	12.165	16.266	15.748	17.648	14.992	0.811
	04	15.015	16.258	15.998	17.671	15.012	1.000
	05	13.459	16.270	15.777	17.691	15.029	0.896
	Avg.	13.131	16.255	15.763	17.659	15.002	0.875
S	01	12.376	16.065	–	17.410	14.789	0.837
	02	12.837	15.711	–	17.027	14.462	0.888
	03	14.306	16.113	–	17.462	14.833	0.964
	04	13.280	15.980	–	17.318	14.710	0.903
	05	13.699	16.129	–	17.480	14.489	0.923
	Avg.	13.300	16.000	–	17.340	14.729	0.903
T	01	12.903	15.867	–	17.196	14.606	0.883
	02	12.937	15.576	–	16.882	14.338	0.902
	03	13.717	16.198	–	17.554	14.912	0.920
	04	13.044	16.056	–	17.401	14.781	0.880
	05	13.298	15.782	–	17.104	14.528	0.915
	Avg.	13.172	15.863	–	17.192	14.603	0.900

<sup>a</sup> No results available because these specimens were used to initially finetune the test setup (A01, A02, B01) or because of technical problems (C1, D2, E3, G1).

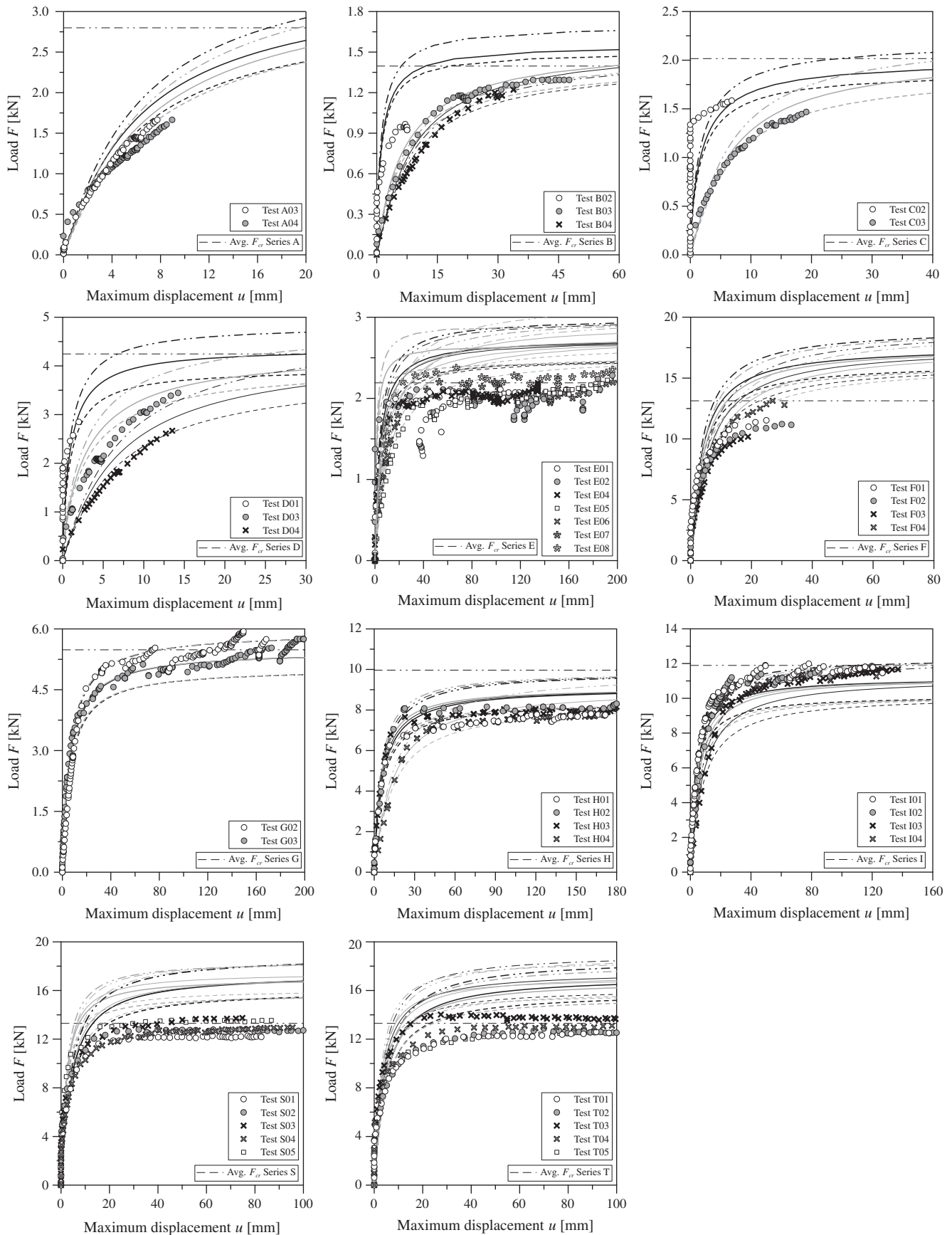


**Fig. D.1.** Further correspondences between experimental load–displacements paths and analytical predictions. Continuous plots are used for nominal glass thickness; dot-line plots for glass thickness with positive tolerance (Tol+); dot plots for glass thickness with negative tolerance (Tol–). Series J and specimens G03, C04, F05 are omitted here as they were already presented in detail in Section 4.2.

## Acknowledgements

Dr. ir. Fred Veer and ir. Mark Feijen are acknowledged for their help in obtaining glass specimens. BRS (NL) and van Noordenne Groep (NL) (in alphabetical order) are gratefully acknowledged for their support. COST Action TU0905 “Structural Glass – Novel Design Methods and Next Generation Products” is gratefully acknowledged for providing an excellent research network and funding for a short term scientific mission of the second author.

## Appendix A

See Table A.1.

## Appendix B

See Table B.1.

## Appendix C

See Table C.1.

## Appendix D

See Fig. D.1.

## References

- [1] Liess J. Bemessung druckbelasteter Bauteile aus Glas. Kassel: Books on Demand GmbH, Universität Kassel; 2001.
- [2] Luible A. Stabilität von Tragelementen aus Glas. Lausanne: Ecole Polytechnique Fédérale de Lausanne; 2004.
- [3] Belis J. Kipsterkte van monolithische en gelamineerde glazen liggers. Ghent: Ghent University; 2005.
- [4] Kasper R. Tragverhalten von Glasträgern. Aachen: Shaker Verlag GmbH, RWTH Aachen; 2005.
- [5] Blauwendraad J. Buckling of laminated glass columns. *Heron* 2007;52(1/2):147.
- [6] Enghardt O. Flächentragwerke aus Glas – Tragverhalten und Stabilität. Vienna: Universität für Bodenkultur Vienna; 2007.
- [7] Mocibob D. Glass panels under shear loading – use of glass envelopes in building stabilization. Lausanne: Ecole Polytechnique Fédérale de Lausanne; 2008.
- [8] Lindner J, Holberndt T. Zum Nachweis von stabilitätsgefährdeten Glasträgern unter Biegebeanspruchung. *Stahlbau* 2006;75(6):488.
- [9] Blauwendraad J. Buckling of laminated glass columns. Comparison and replacement. In: Bos F, Louter PC, Veer F, editors. *Challenging Glass*. Amsterdam: IOS Press BV; 2008. p. 323–8.
- [10] Belis J, Mocibob D, Luible A, Vandebroek M. On the size and shape of initial out-of-plane curvatures in structural glass components. *Constr Build Mater* 2011;25(5):2700–13.
- [11] Timoshenko Stephen P, Gere James M. *Theory of elastic stability*. second ed. New York, Toronto, London: McGraw-Hill Book Company, Inc. Tokyo: Kogkusha Company Ltd.; 1961.
- [12] Roik K, Carl J, Lindner J. *Biegetorsionsprobleme gerader dünnwandiger Stäbe*. Berlin. München. Düsseldorf: Verlag von Wilhelm Ernst & Sohn.; 1972.
- [13] Trahair NS. *Flexural-torsional buckling of structures*. London: E & FN Spon; 1993.
- [14] Southwell RV. On the analysis of experimental observations in problems of elastic stability. *Proc R Soc Lond Ser A* 1932; 135.
- [15] Ariaratnam ST. The Southwell method for predicting critical loads of elastic structures. *Quart J Mech Appl Math* 1961;14(2).
- [16] Lagae G, Paridaens R. Toepasbaarheid van de Southwell-plot op een gelijktijdig knik-kip-verschijnsel van een ligger. *Rijksuniversiteit Gent. Laboratorium voor Modelonderzoek*. Gent; 1982.
- [17] NBN EN 1993-1-1 ANB:2010. Eurocode 3: design of steel structures – Part 1-1: general rules and rules for buildings – National annex. NBN; 2010.
- [18] Amadio C, Bedon C. Analytical approaches for buckling verification of in-plane loaded laminated glass columns and panels. In: Bos, Louter, Nijssse, Veer, editors. *Proceedings of challenging glass 3-conference on architectural and structural applications of glass*, TU Delft, 28 and 29 June 2012. p. 373–86.
- [19] Amadio C, Bedon C. Buckling of laminated glass elements in out-of-plane bending. *Eng Struct* 2010;32:3780–8.
- [20] Kasper R, Sedlacek G, Feldmann M. *Das Biegedrillknickverhalten von Glasträgern aus Verbundglas*. Ernst & Sohn; 2007. Verlag für Architektur und technische Wissenschaften GmbH & Co. KG, Berlin. *Stahlbau* 76; 2007, Heft 3.
- [21] Van Duser A, Jagota A, Bennison S. Analysis of glass/polyvinyl butyral laminates subjected to uniform pressure. *J Eng Mech – ASCE* 1999;125(4): 435–8.
- [22] EN 572-8: 2004. *Glass in building: basic soda lime silicate glass products – part 8: supplied and final cut sizes*. CEN; 2004.